Fusion Engineering and Design 100 (2015) 406–418

Contents lists available at ScienceDirect

Fusion Engineering and Design

journal homepage: www.elsevier.com/locate/fusengdes

Subcooled flow boiling heat transfer of water in a circular tube under high heat fluxes and high mass fluxes

Jianguo Yan [a], Qincheng Bi [a], Zhaohui Liu [a,*], Ge Zhu [a], Laizhong Cai [b]

[a] State Key Laboratory of Multiphase Flow in Power Engineering, Xi'an Jiaotong University, No. 28 Xianning West Road, Xi'an 710049, China
[b] Southwestern Institute of Physics, P.O. Box 432, Chengdu 610041, China

ARTICLE INFO

Article history:
Received 17 March 2015
Received in revised form 3 June 2015
Accepted 2 July 2015
Available online 13 July 2015

Keywords:
Heat transfer
Subcooled flow boiling
High heat flux
High mass flux
ITER

ABSTRACT

Subcooled flow boiling under high heat flux and high mass flux (HHHM) conditions is commonly encountered in nuclear power engineering, for example, the heat removal technology for divertors in the International Thermonuclear Experimental Reactor (ITER). In the present study, subcooled flow boiling heat transfer of water was carried out experimentally in a uniformly heated vertical circular tube with an inner diameter of 9.0 mm under HHHM conditions. Heat transfer coefficients were presented from single-phase convection to fully developed nucleate boiling. The effects of parameters, including mass flux (G = 6000, 8000, and 10,000 kg/m^2 s), heat flux (q = 5–12.5 MW/m^2), system pressure (P = 3, 4.2, and 5 MPa), and thermodynamic vapor quality (x_{th} = −0.5 to −0.03), were discussed. Many previous heat transfer correlations available in the literature were assessed against our experimental data. Most of these correlations cannot predict the experimental data very well. A modified Chen correlation was developed, which predicted the total heat transfer coefficients with a mean average error of 1.11% and a root-mean-square error of 6.45%. A modified Lahey model was proposed to determine the contribution of nucleate boiling in the total heat transfer coefficient under HHHM conditions.

© 2015 Elsevier B.V. All rights reserved.

1. Introduction

Subcooled boiling is characterized by the appearance of bubbles initiating from the heater surface while the bulk temperature is still below the saturation. During subcooled flow boiling, a high heat flux can be obtained with a relatively low wall superheat. Compared to saturated flow boiling, subcooled boiling has higher heat transfer efficiency and better critical heat flux (CHF) performance, which have been confirmed by many previous experimental investigations [1,2]. As a result, subcooled boiling has a wide range of industrial applications, especially in nuclear power reactors.

In recent years, the subcooled boiling under HHHM conditions has been attracting much interest owing to the heat removal technology for divertors in the International Thermonuclear Experimental Reactor (ITER). These divertors can be subjected to extremely high-energy fluxes of up to 10 MW/m^2 from the plasma. Under the current design, subcooled water is used as a coolant for the ITER divertors, and various flow configurations have been proposed, for example, twisted-tape inserts in circular channels and hypervapotron for rectangular channels [3–5]. Although the actual cooling process in these configurations is much more complex, the fundamental mechanism of heat transfer is subcooled flow boiling of water.

Fig. 1 illustrates a typical pattern of subcooled flow boiling under HHHM conditions. The location A with occurrence of initial bubbles denotes the onset of nucleate boiling (ONB). The location B is called the onset of significant void (OSV), where the amount of vapor increases significantly. The location C is known as the fully developed boiling (FDB), where nucleate boiling is fully developed, and the wall temperature almost remains constant. The region between A and C is called the partially boiling (PB) which is the transitional region between the single phase (SP) and FDB. The location D is known as the departure from nucleate boiling (DNB), where the heating surface is covered by too much bubbles, and the wall temperature increases dramatically because of a sharp increase in heat-transfer resistance. In this study, the heat transfer before DNB is focused, especially the heat transfer correlations in the regions of PB and FDB.

In the open literature, many correlations have been proposed for subcooled water flow boiling heat transfer over a wide range of conditions. These correlations serve a useful purpose in the corresponding engineering applications and can be broadly classified into two categories: empirical correlations and mechanism-based correlations. The empirical correlations are usually obtained from

* Corresponding author.
E-mail address: zh_liu@mail.xjtu.edu.cn (Z. Liu).

http://dx.doi.org/10.1016/j.fusengdes.2015.07.007
0920-3796/© 2015 Elsevier B.V. All rights reserved.

Nomenclature

Bo	boiling number
d	diameter, m
f	friction factor
F	enhancement factor
G	mass flux, kg/(m^2 s)
h	heat transfer coefficient, kW/(m^2 K)
H	enthalpy, J/kg
H_{fg}	latent heat of vaporization, J/kg
Ja	Jacob number
L	length, m
L_{eff}	effective heating length, m
M	mass flow, kg/s
Nu	Nusselt number
P	pressure, MPa
Pr	Prandtl number
q	heat flux, MW/m^2
Re	Reynolds number
S	suppression factor
T	temperature, °C
ΔT_b	$T_w - T_b$, °C
ΔT_{sat}	$T_w - T_{sat}$, surface superheat, °C
ΔT_{sub}	$T_{sat} - T_b$, liquid subcooling, °C
x_{th}	thermodynamic vapor quality

Greek symbols

η	thermal efficiency, %
λ	thermal conductivity, W/(m K)
μ	dynamic viscosity, kg/(m s)
ν	kinematic viscosity, m^2/s
ρ	density, kg/m^3
σ	surface tension, N/m

Subscripts

b	bulk
cal	calculated
exp	experimental
fc	forced convection
fdb	fully developed boiling
g	gas
i	inner, inlet
l	liquid
nb	nucleate boiling
o	outer, outlet
ONB	onset of nucleate boiling
OSV	onset of significant void
pb	pool boiling
sat	saturation
sp	single-phase
sub	subcooling
tp	two-phase
w	wall

the fitting of subcooled boiling curves and give an explicit relationship between several parameters, for example, $q = f(\Delta T_{sat})$. However, the application ranges of these empirical correlations are usually limited, and few of them can be consistent with the ITER's requirement. Therefore, they cannot be applied in new situations without further assessments. The mechanism-based correlations attempt to describe the behavior of bubbles and try to connect the macroscopic boiling phenomena with the microscopic process of heat and mass transport. However, the last few decades have not witnessed much success of these correlations developed by various models due to the complexity of boiling phenomenon.

Table 1
Experimental conditions.

Experimental conditions	Characteristics
Heating mode	Electrically heated
Heating power (preheater)	<430 kW
Heating power (test section)	<180 kW
Heat flux	5–12.5 MW/m^2
Inlet bulk temperature	50–200 °C
Mass flux	6000–10,000 kg/(m^2 s)
Pressure	3–5 MPa

Hata et al. [6–8] systematically measured the steady state nucleate boiling heat transfer of subcooled water flow boiling under HHHM conditions in both horizontal and vertical circular tubes. A number of FDB heat transfer correlations were compared with their experimental data. Empirical heat transfer correlations for FDB were derived from corresponding boiling curves.

El-Morshedy and Hassanein [9,10] developed a mathematical model to simulate the thermal hydraulics of the ITER divertor module under conditions of steady and transient states. The Chen correlation [11] was extended to calculate the heat transfer coefficient in subcooled boiling. Their model was validated by experimental data performed for both plain and twisted-tape coolant channel mockups during both steady and transient states.

Ying et al. [12] addressed a 3D CFD simulation to study the subcooled flow boiling heat transfer with hypervapotron configurations for the ITER first wall designs. They used the Bergles–Rohsenow correlation to mark the transition from forced convection to nucleate boiling and the Thom correlation for the prediction of nucleate boiling heat flux.

Kaya et al. [13] studied the boiling heat transfer of water in microtubes at high mass fluxes. In their experiments, ultra-high heat flux (>100 MW/m^2) was obtained at high mass fluxes (>10,000 kg/m^2 s). They also discussed the effects of mass flux, heat flux, local quality, and tube diameter on heat transfer coefficients. Cikim et al. [14] studied the flow boiling in microtubes with cross-linked surface coatings at mass fluxes of 5000 and 20,000 kg/(m^2 s). They observed that heat transfer performance was significantly improved by the porous structure.

Although many studies have been conducted on the subcooled water flow boiling under HHHM conditions, most of them were carried out experimentally in mini or micro channels or by numerical simulations. Experimental studies on the subcooled water flow boiling in conventional channels under HHHM conditions are still insufficient due to rather high experimental requirements, mainly the large heating capacity (typically 1 MW) and high pumping capacity (typically 5000 kg/h). In this study, we investigated the heat transfer of subcooled water flow in a uniformly heated vertical circular tube under the parameter conditions required by the ITER. The experimental conditions are shown in Table 1. The objective of this study is to develop a database, assess the existing heat transfer correlations against our experimental data, and then propose a new correlation for subcooled water flow boiling under HHHM conditions.

2. Literature review on subcooled flow boiling heat transfer correlations

2.1. Empirical heat transfer correlations for FDB

The empirical heat transfer correlations for FDB are generally obtained from a curve fitting method. This type of correlation usually gives an explicit functional relationship between the wall superheat and parameter factors, in the form of $\Delta T_{sat} = f(q, P, G,$

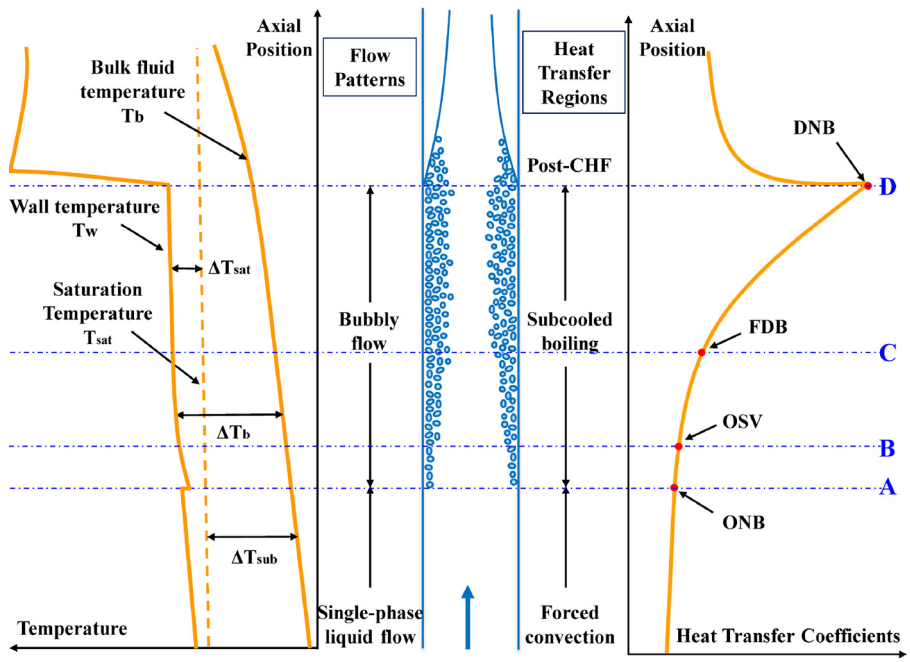

Fig. 1. Typical subcooled flow boiling under high heat fluxes and high mass fluxes.

ΔT_{sub}). The early correlations only took into account the effects of heat flux and pressure. However, later researchers found that the heat transfer in FDB was also affected by mass flux and subcooling. Table 2 lists several empirical heat transfer correlations for FDB.

2.2. Dimensionless correlations

The dimensionless numbers that govern the heat transfer in subcooled boiling region are mainly the boiling number (Bo), Jacob number (Ja), Prandtl number (Pr), and density ratio (ρ_l/ρ_g). The boiling number describes the effect of heat flux and mass flux, the Jacob number represents the effect of subcooling, and the density ratio considers the effect of pressure. Generally, the two-phase Nusselt number is normalized with the single-phase Nusselt number typically calculated from the correlation of Dittus–Boelter or Gnielinski. Therefore, the two-phase heat transfer correlations for subcooled flow boiling can be expressed as a function of $Nu_{tp}/Nu_l = f(Bo, Ja, Pr, \rho_l/\rho_g)$. Table 3 summarizes several dimensionless heat transfer correlations that have been chosen to be assessed in the present study. Note that these correlations are applicable to the whole subcooled boiling region (i.e. both the regions of PB and FDB).

2.3. Chen-type correlations

During the last decades, many models have been developed to predict the heat transfer coefficient during subcooled flow boiling. The most common approach used in these models is to assume that the total heat transfer coefficient is a combination of the SP forced convection and pool nucleate boiling heat transfer coefficients.

Rohsenow [15] first used the combination method and suggested the total subcooled heat transfer coefficient in form of a simple addition of the two components.

$$h_{tp} = h_{fc} + h_{pb} \tag{1}$$

Chen [11] redeveloped the Rohsenow correlation and proposed a model that is generally believed as one of the best correlations for saturated and subcooled flow boiling [16,17]. The Chen correlation is expressed as:

$$h_{tp} = F \cdot h_{fc} + S \cdot h_{pb} \tag{2}$$

$$h_{fc} = 0.023 Re_l^{0.8} Pr_l^{0.4} \frac{\lambda_l}{d} \tag{3}$$

$$h_{pb} = 0.00122 \frac{\lambda_l^{0.79} c_{p,l}^{0.45} \rho_l^{0.49}}{\sigma^{0.5} \mu_l^{0.29} H_{fg}^{0.24} \rho_g^{0.24}} \Delta T_{sat}^{0.24} \Delta P_{sat}^{0.75} \tag{4}$$

Table 2
Empirical heat transfer correlations for fully developed subcooled flow boiling.

Authors	Correlations	Application ranges
Jens and Lottes [45]	$\Delta T_{sat} = 25 q^{0.25} e^{-P/6.2}$	Water, $P = 0.7$–17.2 MPa, $q < 12.5$ MW/m^2, $T_b = 115$–$340\,^\circ$C
Thom et al. [29]	$\Delta T_{sat} = 22.65 q^{0.5} e^{-P/8.7}$	Water, $P < 20$ MPa
Labuntso [46]	$\Delta T_{sat} = \frac{1-0.0045P}{3.4P^{0.18}} (q \times 10^6)^{0.3}$	–
Shah [31]	$q = [230 h_{fc} (G \cdot H_{fg})^{-0.5} \Delta T_{sat}]^2$ where h_{fc} from the Dittus–Boelter equation	Water, refrigerants
Kandlikar [32]	$q = [1058 h_{fc} \Delta T_{sat} (G \cdot H_{fg})^{-0.7}]^{1/0.3}$ where h_{fc} from the Gnielinski equation	Water, refrigerants
Hata and Masuzaki [7]	$q = 51.25 \times 10^{-6} \Delta T_{sat}^3$	Water, SS304 tube
Yagov and co-workers [30]	$q = \frac{0.47 \times 10^{-10} \lambda_l^2 \Delta T_{sat}^3}{\nu_l \sigma_l T_{sat}} \times (1 + \sqrt{1 + 800B} + 400B)$ $B = \frac{H_{fg}}{\sigma_l} \sqrt{\frac{(\nu_l \rho_g)^3}{\lambda_l T_{sat}}}$	Water, $P = 0.4$–2.0 MPa $G = 10^3$–5×10^4 kg/(m^2 s)

Table 3
Dimensionless heat transfer correlations for subcooled flow boiling.

Authors	Correlations	Application ranges
Papel [33]	$\frac{Nu_{tp}}{Nu_l} = 90Bo^{0.7}Ja^{-0.84}\left(\frac{\rho_g}{\rho_l}\right)^{0.7}$	Water, d = 7.9 mm G = 1120–3314 kg/(m^2 s) q = 1.33–2.62 MW/m^2 P = 0.26–1.25 MPa
Badiuzzaman [34]	$\frac{Nu_{tp}}{Nu_l} = 178Bo^{0.75}Ja^{-0.9}\left(\frac{\rho_g}{\rho_l}\right)^{-0.06}\left(\frac{\Delta T_{sub}}{T_{sat}}\right)^{0.45}$	–
Moles and Shaw [35]	$\frac{Nu_{tp}}{Nu_l} = 78.5Bo^{0.67}Ja^{-0.5}\left(\frac{\rho_g}{\rho_l}\right)^{-0.03}Pr^{0.45}$	–
Baburajan et al. [36]	$\frac{Nu_{tp}}{Nu_l} = 267Bo^{0.86}Ja^{-0.6}Pr^{0.23}$	d = 5.5, 7.5, and 9.5 mm G = 450–935 kg/(m^2 s) $\Delta T_{sub,in}$ = 29, 50, and 70 °C

where h_{fc} is the "all liquid" convective heat transfer coefficient calculated by the Dittus–Boelter correlation, and h_{pb} is the pool boiling heat transfer coefficient that takes the modification of Forster and Zuber [18]. The parameter F is called enhancement factor that accounts for the enhancement of forced convection heat transfer due to the presence of vapor. The parameter S is known as suppression factor that takes into account that the correlations of pool boiling overpredict the actual nucleate boiling.

For subcooled flow boiling, the effect of gas-phase is negligible compared to that in saturation boiling. Hence, Eq. (2) can be rewritten as Eq. (5), and the parameters F and S are calculated using Eq. (6).

$$h_{tp} = F \cdot h_{fc} + S \cdot h_{pb} \cdot \frac{T_w - T_{sat}}{T_w - T_b} \tag{5}$$

$$F = 1$$
$$S = \frac{1}{1 + 2.53 \times 10^{-6} Re_l^{1.17}} \tag{6}$$

Gungor and Winterton [19] modified the Chen correlation by introducing the dependence on the boiling number (Bo) and the Martinelli parameter (X_{tt}) in the enhancement factor F. They recommended using the Cooper correlation [20] for pool boiling heat transfer.

$$h_{pb} = 55\left(\frac{P}{P_{cr}}\right)^{0.12}\left[-\log_{10}\left(\frac{P}{P_{cr}}\right)\right]^{-0.55} M^{-0.5} q^{0.67} \tag{7}$$

where P_{cr} is the critical pressure, and M is the molecular weight. For subcooled flow boiling, they also recommended that F equals 1 since there is no net vapor generation, and that S is obtained from Eq. (8).

$$S = \frac{1}{1 + 1.15 \times 10^{-6} E^2 Re_l^{1.17}}$$
$$E = 1 + 24000Bo^{1.16} + 1.37\left(\frac{1}{X_{tt}}\right)^{0.86} \tag{8}$$
$$X_{tt} = \left(\frac{1-x}{x}\right)^{0.9}\left(\frac{\rho_g}{\rho_l}\right)^{0.5}\left(\frac{\mu_l}{\mu_g}\right)^{0.1}$$

Liu and Winterton [21] proposed a power-type addition model for the prediction of subcooled flow boiling heat transfer. Their experiments were carried out in tubes and annuli and covered a range of G = 12.4–8180 kg/(m^2 s), P = 0.05–20 MPa, and ΔT_{sub} = 0–173 °C. The correlation for subcooled flow boiling heat transfer coefficient is expressed as:

$$h_{tp} = \sqrt{(F \cdot h_{fc})^2 + \left(S \cdot h_{pb} \cdot \frac{T_w - T_{sat}}{T_w - T_b}\right)^2} \tag{9}$$

where h_{fc} is calculated using Eq. (3), h_{pb} is determined by Eq. (7), F equals 1, and S is calculated as:

$$S = \frac{1}{1 + 0.055F^{0.1}Re_l^{0.16}} \tag{10}$$

3. Experimental descriptions

3.1. Test loop

The heat-transfer experiments were performed in a high-temperature high-pressure steam-water test loop, as shown in Fig. 2. Deionized feed water from a water tank was driven through a filter by a high-pressure-plunge-type pump with a maximum operating pressure of 40 MPa. Part of the water was returned to the feed water tank through a bypass, and the rest part was pumped through a mass flow meter into a regenerative exchanger and then a preheater, in which the water was heated to the desired properties by electrical AC power supplies. The water then flowed into the test section. After that, the water flowed through the regenerative exchanger and a condenser, in which the heat absorbed in the test section was extracted. The water was sent back to the water tank and recirculated after cooled down. A throttle valve (adjacent to the main valve) was installed upstream of the heating sections to suppress potential boiling instabilities.

3.2. Test section

The experiments were performed in a vertical circular nickel alloy tube with an upward water flow. A detailed diagram of the test tube is presented in Fig. 3. The tube was uniformly heated using electrical AC power with a maximum capacity of 250 kW. The inner diameter, outer diameter, and effective heating length of the test tube were 9.0, 12.0, and 400 mm, respectively. Tube-fittings and ferrules (manufactured by Swagelok) were used to seal and connect the test tube to the whole system. At each end of the test tube, there was a non-heated tube (L = 300 mm, d_i = 9.0 mm) to avoid the flow entrance effect and stabilize the fluid flow. The inner surface roughness (Ra) of the test tube was obtained as 1.376 μm using a roughness measuring instrument (PGI Optics 3D, manufactured by Taylor Hobson).

3.3. Parameter measurements

The measured parameters mainly include the mass flow (M), inlet pressure (P), pressure drop (dP), power applied ($Power$), bulk temperatures (T_b), and outer wall temperatures ($T_{w,o}$).

M was measured using a Coriolis mass flow meter (manufactured by Siemens). P and dP were determined by a

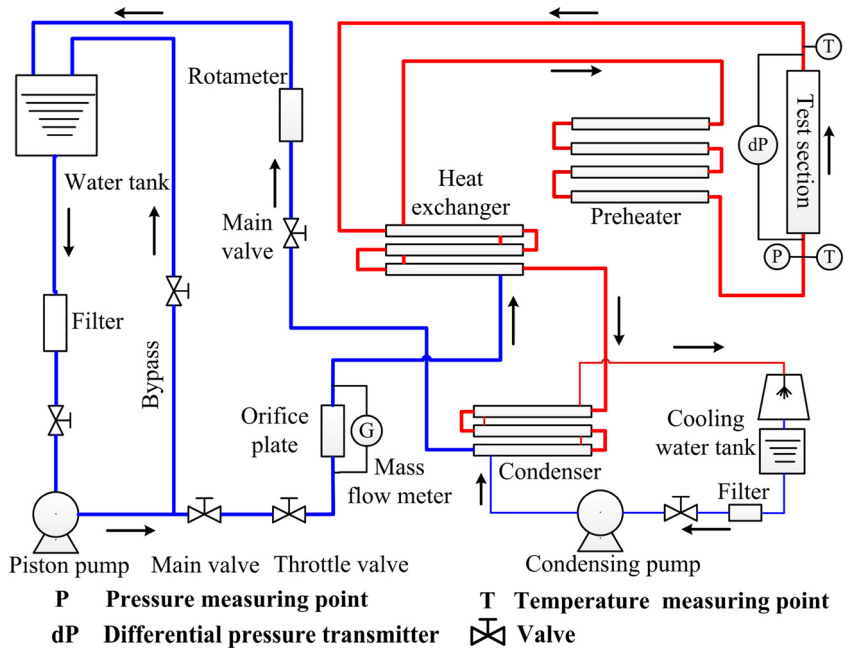

Fig. 2. Schematic diagram of the test loop.

Rosemount-3051 pressure transmitter and a Rosemount-3051 differential pressure transducer, respectively. The power applied to the test tube was obtained by multiplying the voltage by the current, which were measured by relevant transformers and transducers.

T_b was measured by Φ 1.5-mm K-type sheathed thermocouples (TCs) at the inlet and outlet of the test tube. $T_{w,o}$ was obtained using eight K-type TCs welded onto the outside surface of the tube with a 50-mm uniform spacing. In addition, at the location of TC8, four TCs were arranged uniformly in a circumferential pattern to monitor a possible soaring wall temperature. The detailed arrangement of the TCs is also shown in Fig. 3. In order to guarantee the thermal efficiency and the accuracy of the wall temperature measurement, the test section was wrapped with thermal insulation materials.

All of the measured signals were monitored and recorded by an IMP 3595 distributed data acquisition system (supplied by the UK Solartron).

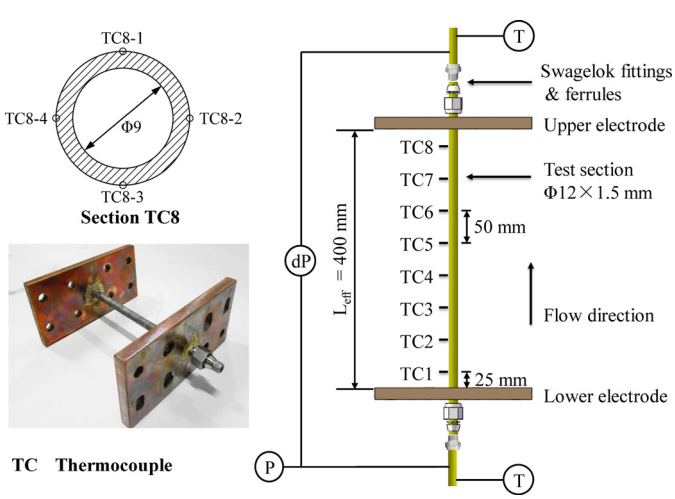

Fig. 3. Details of the test section.

3.4. Experimental procedure

First, a heat balance test was conducted to determine the thermal efficiency of the test section. The thermal efficiency is calculated as:

$$\eta = \frac{M}{Power}(H_{b,o} - H_{b,i}) \tag{11}$$

where $H_{b,i}$ and $H_{b,o}$ are the bulk fluid enthalpy at the inlet and outlet, respectively, and *Power* is the total heating power applied in the test section. In this study, the thermal efficiency was in the range of 93.0–97.0%.

The heat-transfer experiments were carried out under the condition of constant heat flux. In this procedure, the heat flux of the test section was maintained at a constant level (5, 7.5, 10, or 12.5 MW/m^2), and the preheater heating power was gradually increased to heat the water to the desired temperature. After all of the parameters had achieved a steady state, data were collected continuously for approximately 90 s at each working condition.

3.5. Data reduction

The quantities directly measured include the mass flow (M), inlet pressure (P), pressure drop (dP), voltage drop and current (U, I), diameters (d_i, d_o), effective heating length (L_{eff}), bulk temperatures ($T_{b,i}$, $T_{b,o}$), and outer wall temperatures ($T_{w,o}$). The main derived quantities include the mass flux (G), heat flux (q), thermodynamic vapor quality (x_{th}), heat transfer coefficient (h), and the dimensionless numbers (*Bo*, *Ja*, *Re*, *Nu*, etc.). The mass flux and heat flux are determined as:

$$G = \frac{4M}{\pi d_i^2} \tag{12}$$

$$q = \frac{U \cdot I \cdot \eta}{\pi d_i L_{eff}} \tag{13}$$

The thermodynamic vapor quality is calculated as:

$$x_{th} = \frac{H_b - H_{l,sat}}{H_{fg}} \tag{14}$$

Table 4
Uncertainties of the main experimental parameters.

Parameters	Units	Uncertainties
Pressure	MPa	±0.25%
Bulk temperature	°C	±0.5%
Outer wall temperature	°C	±0.4%
Mass flux	kg/(m^2 s)	±0.26%
Heat flux	MW/m^2	±4.87%
Heat transfer coefficient	kW/(m^2 K)	±6.41%

where $H_{l,sat}$ is the saturated liquid enthalpy, and H_{fg} is the latent heat of vaporization. H_b is the local bulk enthalpy and is determined from heat balance:

$$H_b = H_{b,in} + \frac{U \cdot I \cdot \eta}{M} \frac{z}{L_{eff}} \tag{15}$$

where $H_{b,in}$ is the inlet enthalpy, and z is the axial distance from the start of the heated length. The inner wall temperature is obtained from outer wall temperature by solving a heat conduction model of a cylindrical tube assuming uniform heat generation, which was discussed in detail in [22]. The heat transfer coefficient is calculated as:

$$h = \frac{q}{T_{w,i} - T_b} \tag{16}$$

The boiling number and Jacob number are defined as:

$$Bo = \frac{q}{G \cdot H_{fg}} \tag{17}$$

$$Ja = \frac{c_p \Delta T_{sub}}{H_{fg}} \tag{18}$$

where c_p is the specific heat, and ΔT_{sub} is the liquid subcooling. The Reynolds number and Nusselt number are calculated as:

$$Re = \frac{\rho u d_i}{\mu} \tag{19}$$

$$Nu = \frac{h d_i}{\lambda} \tag{20}$$

The thermophysical properties of water are obtained from the NIST REFPROP program.

3.6. Uncertainty analysis

An uncertainty analysis was carried out using the method proposed by Coleman and Steele [23]. According to this method, the relative uncertainties of q and h are calculated as:

$$\frac{\delta q}{q} = \left[\left(\frac{\delta U}{U}\right)^2 + \left(\frac{\delta I}{I}\right)^2 + \left(\frac{\delta \eta}{\eta}\right)^2 + \left(\frac{\delta (d_i)}{d_i}\right)^2 + \left(\frac{\delta L_{eff}}{L_{eff}}\right)^2 \right]^{1/2} \tag{21}$$

$$\frac{\delta h}{h} = \left[\left(\frac{\delta q}{q}\right)^2 + \left(\frac{\delta T_w}{T_w - T_b}\right)^2 + \left(\frac{\delta T_b}{T_w - T_b}\right)^2 \right]^{1/2} \tag{22}$$

According to the above analysis, as well as the calibrations and accuracies of the measuring instruments, the uncertainties of the main parameters were calculated and summarized in Table 4.

4. Results and discussion

Heat-transfer experiments were performed to determine the heat transfer coefficients of subcooled flow boiling of water in a vertical circular tube under HHHM conditions. The effects of G, q, P, and ΔT_{sub} on heat transfer coefficients were discussed. All data were obtained under a fixed G, q, and P; therefore, the results were presented in terms of h vs. T_w or h vs. x_{th}. The boiling curves (i.e. q vs. ΔT_{sat}) were not depicted in this study.

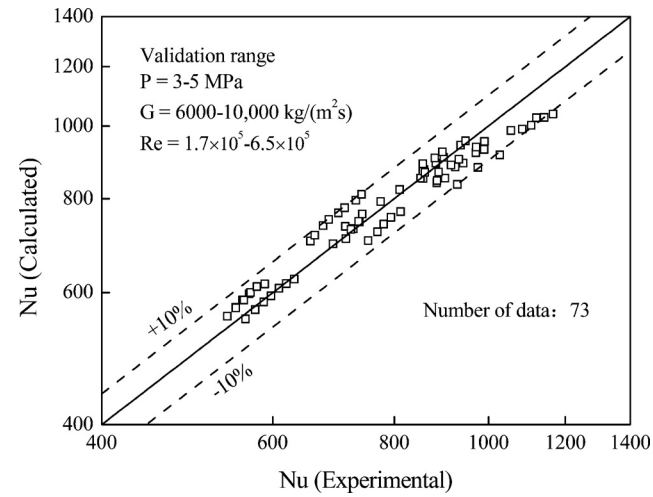

Fig. 4. Validation of the experimental system: comparison of the experimental Nu with the calculated Nu from the Gnielinski equation.

4.1. Validation test

To evaluate the accuracy and reliability of the present experimental system, a validation test was performed. In the validation test, the water flowed into the tube covering a range of P = 3–5 MPa and G = 6000–10,000 kg/(m^2 s). The single-phase Nusselt numbers were obtained and then compared with the predictions of the Gnielinski correlation [24].

$$Nu = \frac{(f/8)(Re_b - 1000)Pr_b}{1 + 12.7\sqrt{f/8}(Pr_b^{2/3} - 1)} \left[1 + (d/L)^{2/3}\right] (Pr_b/Pr_w)^{0.01} \tag{23}$$

where f is the friction factor obtained from the Filonenko correlation.

$$f = (1.82 \ \lg Re_b - 1.64)^{-2} \tag{24}$$

Fig. 4 presents the comparison between the experimental data and the calculated data from the Gnielinski correlation. The results show that the experimental data were in good agreement with the predictions. Most of the data were captured with an accuracy of ±10%. Therefore, the reliability of our experimental system and data processing procedure were validated.

4.2. Effect of mass flux

Fig. 5 shows the effect of mass flux on the heat transfer coefficient of subcooled water flow boiling at P = 4.2 MPa and q = 7.5 MW/m^2. In the SP region, heat transfer is governed by forced convection, and the heat transfer coefficient is essentially a function of mass flux and almost independent of heat flux. For a given x_{th}, a higher G leads to a higher h.

In the region of nucleate boiling, the wall superheat is high enough to initiate formation of bubbles. In the beginning, few nucleation sites are activated, and heat transfer coefficients still show a strong dependence on mass flux. However, with a further increase in x_{th}, the effect of G on h diminishes gradually because of the increase in the contribution of nucleate boiling.

In the region of FDB, the wall temperatures almost remain constant. For a given x_{th}, an increase in G is not coupled with an increase in h. This indicates that the heat transfer is independent of mass flux

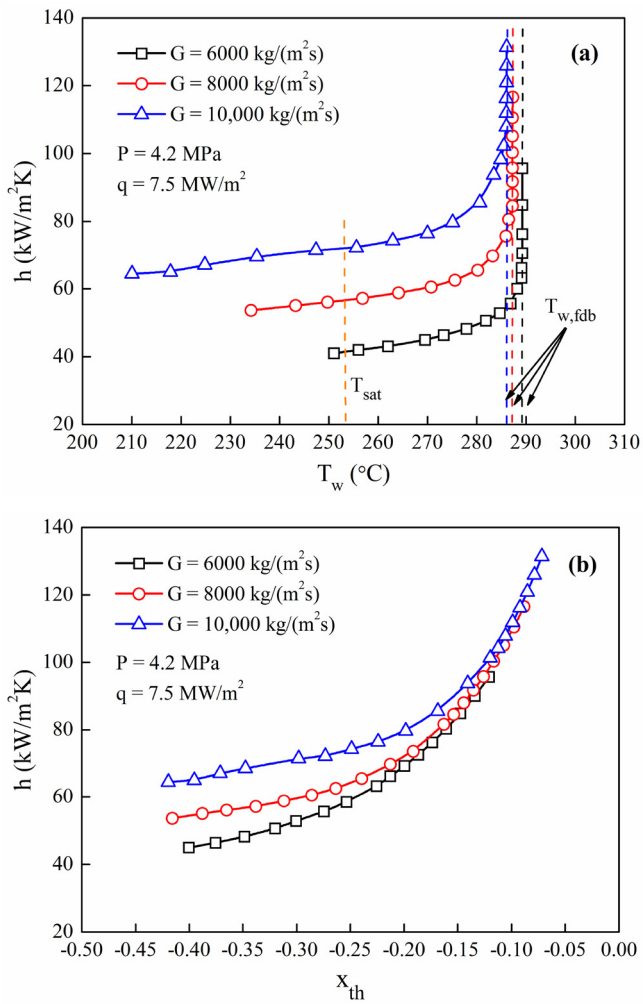

Fig. 5. Effect of mass flux on heat transfer coefficient: (a) h vs. T_w and (b) h vs. x_{th}.

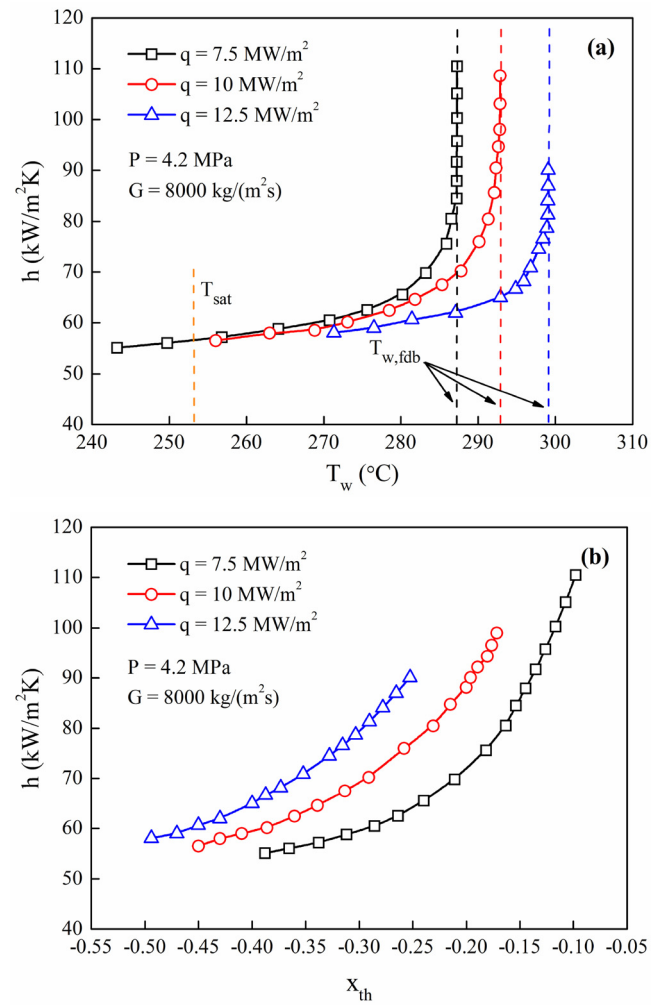

Fig. 6. Effect of heat flux on heat transfer coefficient: (a) h vs. T_w and (b) h vs. x_{th}.

and that the dominant heat transfer mechanism has transformed into nucleate boiling.

4.3. Effect of heat flux

Fig. 6 presents the effect of heat flux on the heat transfer coefficients of subcooled water flow boiling at $P = 4.2$ MPa and $G = 8000$ kg/(m^2 s). Heat transfer coefficient is little affected by heat flux in the SP region. For a given x_{th}, a higher heat flux leads to a higher wall superheat and an earlier generation of bubbles. As heat flux is further increased, more bubbles occur, and the contribution of nucleate boiling continues to rise. In the FDB region, heat transfer coefficients are strongly dependent on heat flux.

Heat flux also affects the wall superheat at ONB and FDB (i.e. $\Delta T_{sat,ONB}$ and $\Delta T_{sat,FDB}$). Both of them increase with increasing heat flux. Many correlations have given the relationship between the wall superheat and heat flux. Generally, $\Delta T_{sat,ONB}$ and $\Delta T_{sat,FDB}$ are both proportional to q^n, where the exponent n differs in different correlations.

4.4. Effect of pressure

Fig. 7 presents the effect of pressure on the heat transfer coefficients of subcooled water flow boiling at $G = 8000$ kg/(m^2 s) and $q = 10$ MW/m^2. The pressure varied from 3 MPa to 5 MPa, and the saturation temperature varied correspondingly from 233.9 °C to 263.9 °C.

It can be observed that pressure has little influence on the heat transfer in the SP region. However, an obvious effect of pressure on heat transfer can be found in the region of subcooled boiling. An increase in pressure improves the heat transfer coefficient, which could be related to the variation in fluid properties under different pressures. An increasing pressure can result in a decreasing surface tension and liquid-to-gas density (ρ_l/ρ_g), which is benefit to the activation of nucleate sites. Similar trends were also reported by Basu et al. [25], Martin-Callizo et al. [26], and Saitoh et al. [27], in their studies with refrigerant R134a during subcooled and saturated flow boiling.

4.5. Effect of subcooling

Effect of subcooling on the heat transfer coefficients of subcooled water flow boiling can be also found in Figs. 5b, 6b, and 7b. The subcooling ΔT_{sub} is defined as the difference between the saturation temperature T_{sat} and the local bulk temperature T_b and can be represented by x_{th}. A larger x_{th} corresponds to a higher T_b and hence a lower ΔT_{sub}.

Under high mass fluxes and low heat fluxes, the effect of subcooling is not obvious because the dominate mechanism of heat transfer is SP forced convection. For a given G and q, heat transfer coefficients increase gradually as subcooling decreases. This trend

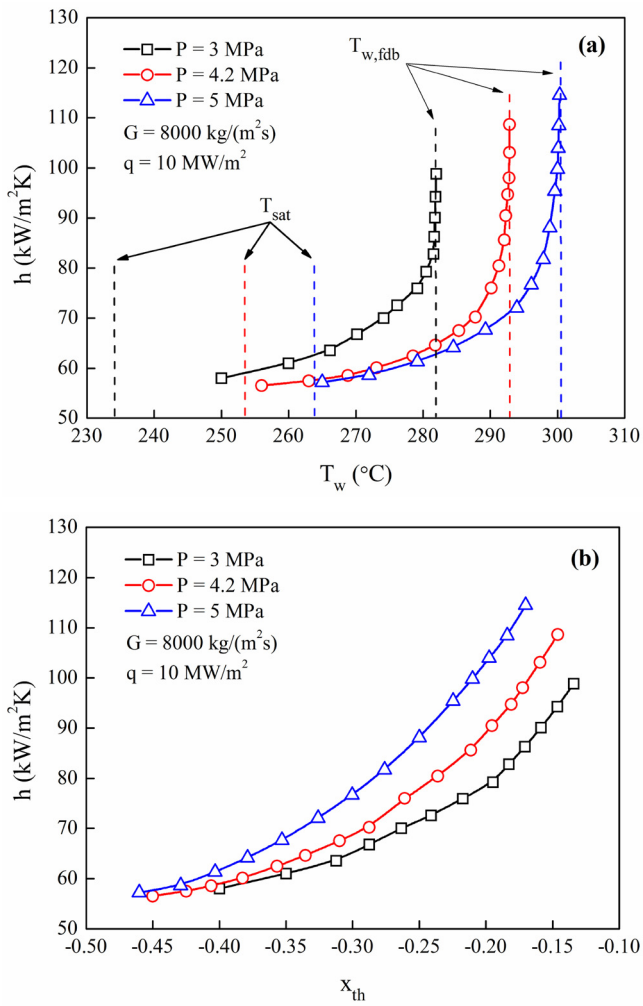

Fig. 7. Effect of pressure on heat transfer coefficient: (a) h vs. T_w and (b) h vs. x_{th}.

can be explained by the variation of the denominator in Eq. (16). The heat-transfer temperature difference ΔT_b can be expressed as:

$$\Delta T_b = T_w - T_b = (T_w - T_{sat}) + (T_{sat} - T_b) = \Delta T_{sat} + \Delta T_{sub} \tag{25}$$

When T_b increases, T_w also increases in the region of subcooled boiling, suggesting an increase in ΔT_{sat} while a decrease in ΔT_{sub}. However, ΔT_{sub} varies more strongly than ΔT_{sat}; therefore, the heat transfer coefficient becomes larger due to the decrease in ΔT_b. In fact, the relationship between ΔT_{sat} and ΔT_{sub} is quite complex and is dependent on many factors in bubble growth mechanisms. More information on the effect of subcooling can be referred to Basu et al. [25] and Jamialahmadi et al. [28].

5. Heat transfer correlations

5.1. Assessment of heat transfer correlations in subcooled water flow boiling

Many correlations have been proposed to predict the heat transfer coefficients in subcooled water flow boiling. However, because of the complexity of boiling heat transfer and two-phase flow, an accurate correlation over a wide range of parameters has not yet been obtained, especially under the conditions of HHHM required by the ITER.

In the present study, a total of 376 data points (PB: 187; FDB: 189) were used to evaluate the existing correlations for subcooled water flow boiling. The prediction performances were

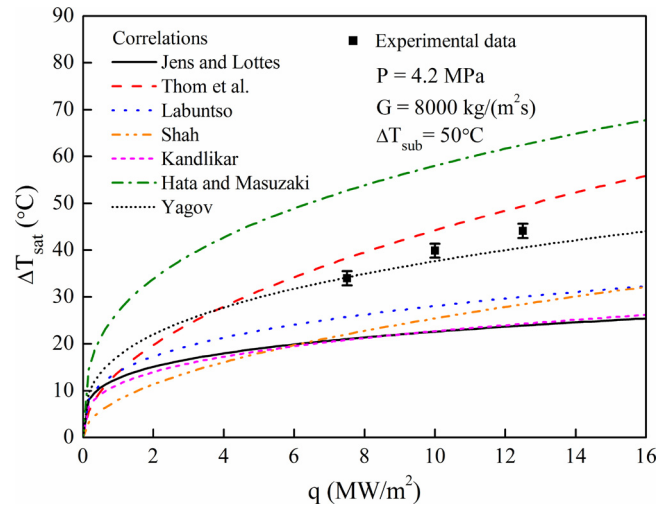

Fig. 8. Comparison of boiling curves using the typical heat transfer correlations for FDB.

quantitatively assessed using the mean average error (MAE) and root-mean-square error (RMSE) defined as:

$$\mathrm{MAE} = \frac{1}{N}\sum_{i=1}^{N}\left(\frac{Nu_{cal} - Nu_{exp}}{Nu_{\exp}}\right) \times 100\% \tag{26}$$

$$\mathrm{RMSE} = \sqrt{\frac{1}{N}\sum_{i=1}^{N}\left(\frac{Nu_{cal} - Nu_{exp}}{Nu_{\exp}}\right)^2} \times 100\% \tag{27}$$

where N is the number of experimental data.

5.1.1. Empirical heat transfer correlations for FDB

Fig. 8 shows the comparison of the experimental $\Delta T_{sat,fdb}$ with the predictions using the correlations in Table 2 under the condition of $P = 4.2$ MPa, $G = 8000$ kg/(m^2 s), and $\Delta T_{sub} = 50\,^\circ$C. The results indicate that most of these correlations underpredicted $\Delta T_{sat,fdb}$. However, the estimated values of $\Delta T_{sat,fdb}$ using the correlation of Hata and Masuzaki [7] were much higher than the experimental values. This could be explained by that the correlation of Hata and Masuzaki was developed in tubes with mirror finished surfaces. Based on their results, the FDB is also affected by the roughness of heating surfaces, and a higher wall superheat is needed for a smoother heating surface.

Fig. 9a compares Nu_{exp} with Nu_{cal} in the region of FDB, and Fig. 9b shows the distribution of Nu_{cal}/Nu_{exp} with thermodynamic vapor quality. The results of quantitative assessments for these correlations are listed in Table 5. The results show that the correlations of Thom et al. [29] and Yagov [30] had good agreement with the experimental data with the MAEs of −5.55% and −0.42%, respectively, and the RMSEs of 6.08% and 1.55%, respectively. Nu_{cal} using the two correlations followed the trend of Nu_{exp} in both regions of PB and FDB. The correlations of Shah [31] and Kandlikar [32] consistently overpredicted Nu, and the prediction deviations became larger as x_{th} increased. The poor results of the correlations of Shah and Kandlikar in the zone of FDB were expected due to the strong relationship between ΔT_{sat} and h_{fc}. The correlations of Hata and Masuzaki did not well capture our experimental data, and its MAE and RMSE were −16.76% and 17.48%, respectively, which may be due to the different surface roughness of test tubes.

5.1.2. Dimensionless correlations

Fig. 10a shows the comparison of the experimental Nu with the calculated Nu using the dimensionless correlations (see Table 3).

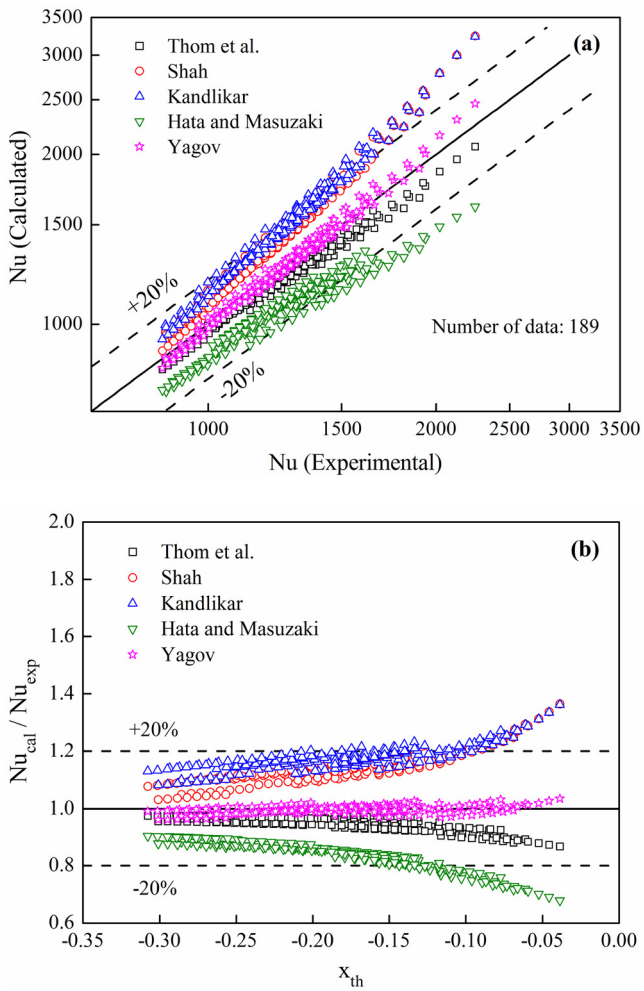

Fig. 9. Prediction performances of the heat transfer correlations for FDB: (a) Nu_{cal} vs. Nu_{exp} and (b) Nu_{cal}/Nu_{exp} vs. x_{th}.

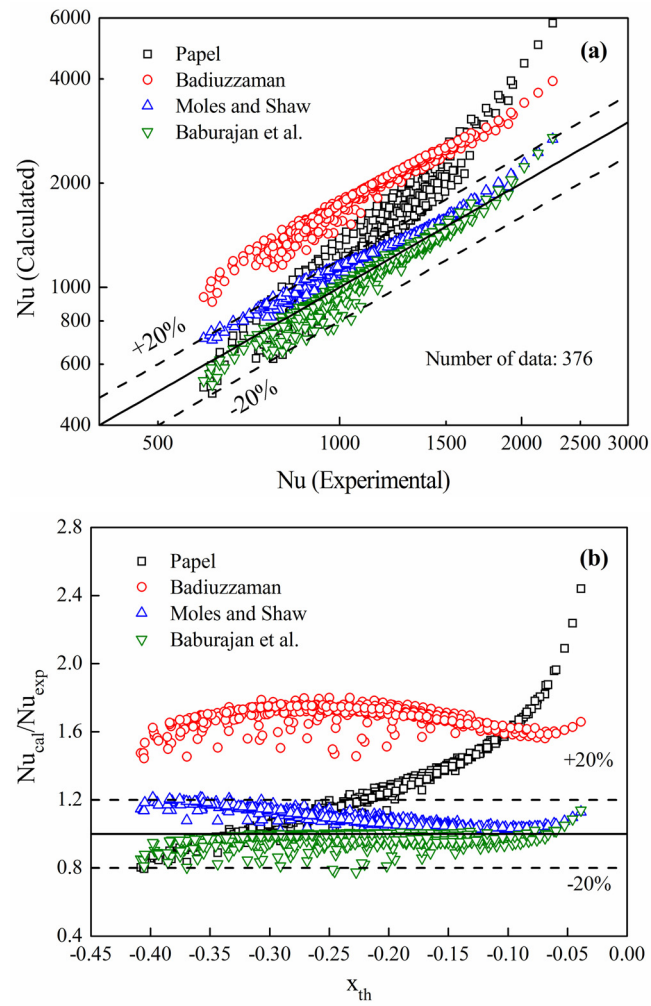

Fig. 10. Prediction performances of the dimensionless heat transfer correlations: (a) Nu_{cal} vs. Nu_{exp} and (b) Nu_{cal}/Nu_{exp} vs. x_{th}.

The variation of Nu_{cal}/Nu_{exp} with x_{th} is presented in Fig. 10b. The prediction performance of the four correlations can be found in Table 5.

The Papel correlation [33] predicted the Nusselt number well near the ONB, but its prediction accuracy deteriorated with increasing x_{th}. The correlation failed to capture the heat transfer data in the region of FDB, especially when x_{th} approached zero. The MAE and RMSE for the Papel correlation were 21.81% and 32.48%, respectively. It may be because the effect of Jacob number is too strong in the region of FDB (i.e. the value of n in Ja^{-n} is too great).

The Badiuzzaman correlation [34] consistently overpredicted the experimental data by approximately 70%, but the prediction trend corresponded with the experimental trends. The reason may be that the correlation was applied beyond its recommended ranges in the present study.

The correlation of Moles and Shaw [35] captured 98.4% of the data with an accuracy of ±20%. Meanwhile, 99.2% of the data can be predicted within ±20% by the correlation of Baburajan et al. [36]. The MAEs for the two correlations were 9.49% and −4.02%, respectively, and the RMSEs were 10.79% and 6.15%, respectively. Moreover, the prediction trends of the two correlations were also good over the whole subcooled region.

Table 5
Comparison of the experimental data with the empirical heat transfer correlations.

Authors	MAE (%)	RMSE (%)	Data inliers		
			20%	30%	40%
Jens and Lottes	18.04	18.31	76.72	99.47	100
Thom et al.	−5.55	6.08	100	100	100
Labuntso	10.83	10.98	100	100	100
Shah	14.33	15.42	86.77	98.41	100
Kandlikar	17.70	18.25	75.66	98.41	100
Yagov	−0.42	1.55	100	100	100
Hata and Masuzaki	−16.76	17.48	77.78	98.94	100
Papel	21.81	32.48	52.93	66.76	81.91
Badiuzzaman	68.49	68.82	0	0	0
Moles and Shaw	9.49	10.79	98.40	100	100
Baburajan et al.	−4.02	6.15	99.20	100	100
Chen	−20.28	22.15	50	84.84	98.67
Gungor and Winterton	−27.59	29.30	25	52.66	90.69
Liu and Winterton	70.0	73.04	4.79	6.38	9.04
Modified Chen	1.11	6.45	100	100	100

5.1.3. Chen-type correlations

The Chen correlation is one of the most famous correlations for flow boiling heat transfer. The correlation adopts an additive model and considers that the mechanisms of two-phase flow boiling are consisted of both forced convection and saturated nucleate boiling. Many researchers have modified the Chen correlation mainly by refining the parameters F and S, for example, the correlations of Gungor–Winterton [19] and Liu–Winterton [21]. In this study, these correlations were grouped as Chen-type correlations.

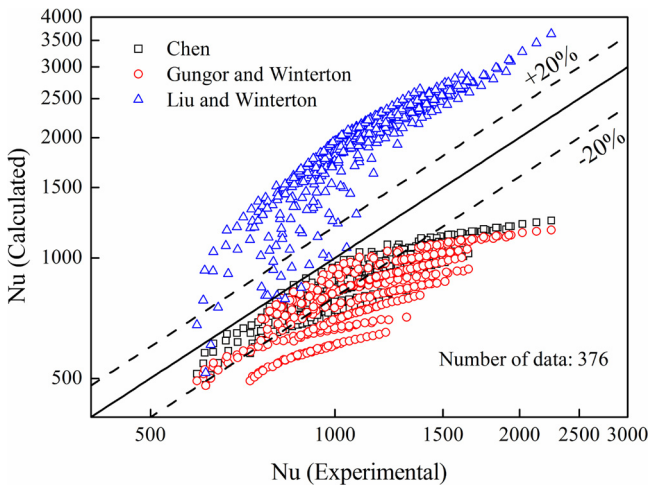

Fig. 11. Comparison of the experimental and predicted *Nu* using the Chen-type correlations.

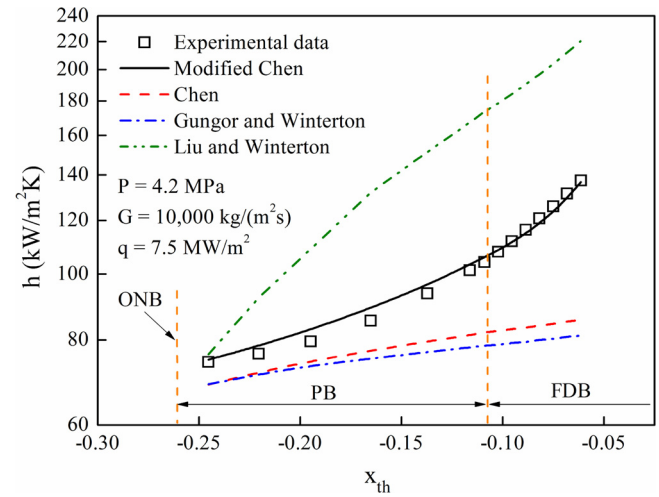

Fig. 12. Comparison of the predicted *h* using the Chen-type correlations.

A detailed description of typical Chen-type correlations is available in Section 2.3.

The Chen-type correlations were proposed initially for saturated flow boiling and later were extended to subcooled flow boiling. However, some researchers have pointed out their poor performance in subcooled flow boiling [37]. In this section, these correlations were assessed using our experimental data obtained in subcooled flow boiling under HHHM conditions.

Fig. 11 compares the experimental *Nu* with predicted *Nu* using the Chen-type correlations. The results show that the Chen correlation and the correlation of Gungor and Winterton both underpredicted *Nu*. The MAEs for the two correlations were −20.28% and −27.59%, respectively. Moreover, they cannot capture the experimental trends, and the deviations became larger with increasing x_{th}. The RMSEs for the two correlations were 22.15% and 29.30%, respectively. The correlation of Liu and Winterton typically overpredicted most of *Nu* with the MAE = 70.0% and RMSE = 73.04%.

For subcooled boiling, the enhancement factor *F* is commonly set to unity; therefore, the prediction accuracies of Chen-type correlations are mainly determined by the suppression factor *S*. According to our results, *S* is too weak in Eqs. (6) and (8) but too strong in Eq. (10) for subcooled flow boiling under HHHM conditions. Therefore, a modified Chen correlation is proposed, in which h_{fc} is calculated using the Gnielinski correlation, *S* is calculated by Eq. (28), and the others remain the same with those in the Chen correlation.

$$S = \frac{1}{1 + 2.53 \times 10^{-6} Re_l^{1.17}} \left(\frac{T_{sat}}{\Delta T_{sub}} \right)^{0.9} \tag{28}$$

Fig. 12 shows the predicted heat transfer coefficient by the four Chen-type correlations at $P = 4.2$ MPa, $G = 10{,}000$ kg/(m^2 s), and $q = 7.5$ MW/m^2. The results show that the modified Chen correlation fit the experimental data well. The prediction *h* followed the trend of the experimental data over the entire subcooled region. Meanwhile, the prediction *h* from the other three correlations varied far from the experimental data, especially in the region with low subcooling, which can be attributed to the variations in the predicted q_{nb}.

Fig. 13 represents the distributions of Nu_{cal}/Nu_{exp} along with x_{th} for the correlations of Chen and modified Chen. Contrasted to the Chen correlation, the modified Chen correlation performed well in the subcooled region near the saturated point. The MAE and RMSE of the modified Chen correlation were 1.11% and 6.45%, respectively, and 97.07% of the data were captured within an error limit of ±15%. The validated range for the modified Chen correlation covers the range of $P = 3$–5 MPa, $G = 6000$–$10{,}000$ kg/(m^2 s), $q = 5$–12.5 MW/m^2, and $x_{th} < -0.03$.

It is noteworthy that the modified Chen correlation was only validated in uniform heating conditions. In the case of the ITER divertors, the cooling tubes are subjected to one-sided heating, in which the distributions of the local wall temperature and heat flux are nonuniform along the circumference of the cooling channel, and thus the heat transfer coefficient should be predicted locally. Therefore, the modified Chen correlation proposed in this study cannot be used directly in one-sided heating applications.

In order to analyze the heat transfer for one-sided heating, one strategy is to adapt and modify the heat transfer correlations originally developed for uniform heating. For example, Araki et al. [38] proposed that heat transfer under one-sided heating conditions can be indicated as a combination of the effects in forced convection and nucleate boiling as follows:

$$q = k \cdot q_{fc} + (1 - k) \cdot q_{nb} \tag{29}$$

where *k* is determined by geometries (mainly the circumferential angle), and q_{fc} and q_{nb} are heat fluxes for forced convection and nucleate boiling, respectively, which are obtained under uniform heating conditions. Their results show that the approach is effective in predicting the local heat transfer.

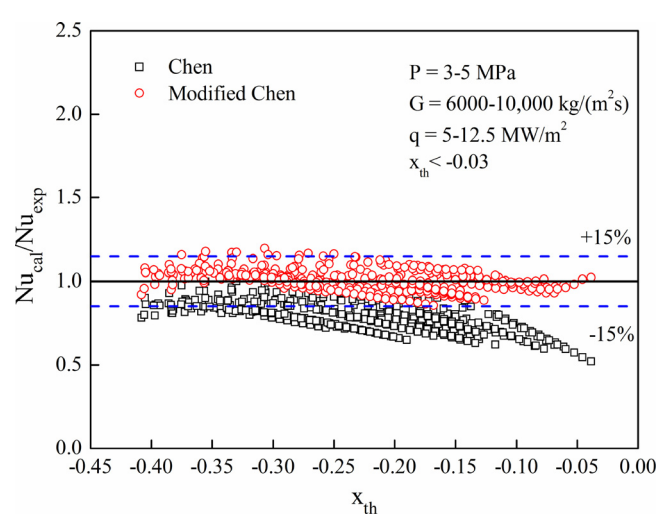

Fig. 13. Distributions of Nu_{cal}/Nu_{exp} along with x_{th} for the correlations of Chen and modified Chen.

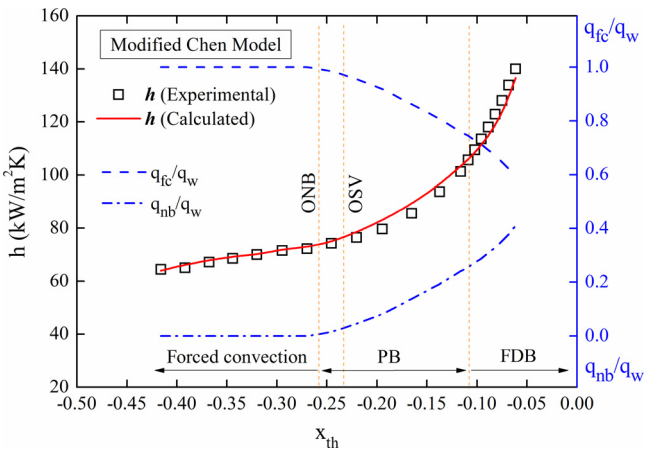

Fig. 14. Heat transfer coefficients and wall heat flux partitioning according to the modified Chen model (P = 4.2 MPa, G = 10,000 kg/m^2 s, q = 7.5 MW/m^2).

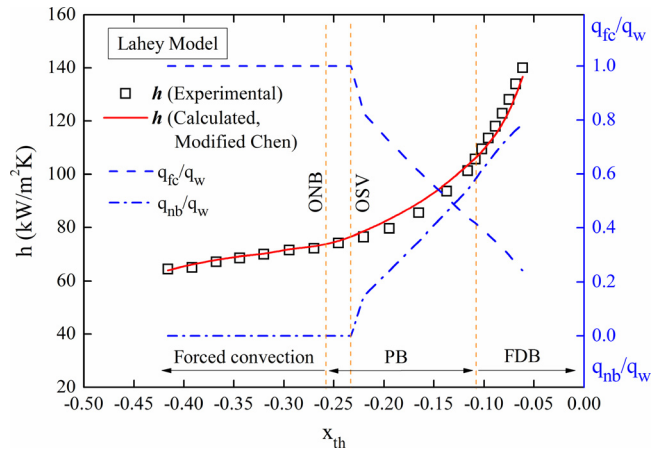

Fig. 15. Wall heat flux partitioning according to the Lahey model (P = 4.2 MPa, G = 10,000 kg/m^2 s, q = 7.5 MW/m^2).

To sum up, although the modified Chen correlation can only be used in uniform heating so far, it can serve as a basic correlation when researchers develop correlations for nonuniform heating. Further modifications, such as taking into account the circumferential angle, are required to obtain heat transfer correlations applicable to one-sided heating conditions.

5.2. Wall heat flux partitioning model

5.2.1. Nucleate boiling fraction

It should be noted that the heat transfer correlations mentioned above (Tables 2 and 3, and Chen-type) are all limited to predict the overall heat transfer coefficient during subcooled flow boiling. However, knowledge of only the overall heat transfer coefficient is insufficient in many industrial applications, such as nuclear reactors. One needs to know how the total wall heat flux is partitioned and what the nucleate boiling fraction (NBF, defined in Eq. (30)) is in the total heat transfer (i.e. the fraction of the total wall heat flux utilized to generate bubbles) because the two-phase thermal hydraulics of nuclear reactors is closely related to the bubble generation.

$$\mathrm{NBF} = \frac{q_{nb}}{q_w} \tag{30}$$

Fig. 14 shows the heat transfer coefficients and the NBF as functions of x_{th} using the modified Chen correlation under the condition of P = 4.2 MPa, G = 10,000 kg/(m^2 s), and q = 7.5 MW/m^2. The results show that the modified Chen correlation can capture the total heat transfer coefficient quite well. However, a significant weakness of the modified Chen can be found when partitioning the wall heat flux. From Fig. 14, the dominant heat transfer is always forced convection, even in the region of FDB, which puts its physical correctness into question. According to Fig. 14, the NBF at FDB was less than 0.4.

It should be noted that the Chen-type correlations all perform poorly with respect to wall heat flux partitioning under our experimental conditions.

5.2.2. Wall heat flux partition

In the open literature, there are several models proposed for the wall heat flux partitioning, for example, models of Griffith et al. [39], Bowring [40], Rouhani–Axelsson [41], and Hancox–Nicoll [42]. Note that the purpose of these correlations is to determine how the wall flux is to be partitioned and not to predict the total wall heat flux itself.

In the present study, the Lahey model, one of the most widely used models in thermal hydraulic codes, is used to predict the wall heat flux partition in our experiments. The model identifies two distinct region: upstream of OSV (region 1) and downstream of OSV (region 2), in which the location of OSV is determined using the correlation of Saha and Zuber [43]. In the region 1, the void fraction is negligible, and NBF = 0 (i.e. $q_w = q_{fc}$). In the region 2, the NBF is expressed as:

$$\mathrm{NBF} = \frac{q_{nb}}{q_w} = 1 - \frac{H_{l,sat} - H_l}{H_{l,sat} - H_{l,OSV}} \tag{31}$$

where $H_{l,OSV}$ is the liquid enthalpy at OSV. Fig. 15 shows the contributions of forced convection and nucleate boiling in the total wall heat flux under the condition of P = 4.2 MPa, G = 10,000 kg/(m^2 s), and q = 7.5 MW/m^2. In Fig. 15, the NBF at the initial of FDB ($x_{th} \approx -0.11$) is approximately 0.6, suggesting that the forced convection and nucleate boiling both play a role in the FDB regime. However, according to the results in Fig. 5b, the heat transfer is actually independent of mass flux, and the actual dominant heat transfer mechanism is nucleate boiling.

The reason for the inconsistency could be that $\Delta T_{sub,fdb}$ under conditions of HHHM is much greater than that under conditions of low heat fluxes and low mass fluxes. Thus, $(H_{l,sat} - H_l)$ cannot be negligible compared to $(H_{l,sat} - H_{l,OSV})$, and then the q_{sp}/q_w at FDB is still pronounced. Therefore, it could be concluded that it is inappropriate to adopt the Lahey model under HHHM conditions.

Here, a modified Lahey model is proposed to predict the NBF in subcooled boiling under HHHM conditions. In the modified model, the NBF is calculated using Eq. (32) instead of Eq. (31).

$$\mathrm{NBF} = \frac{q_{nb}}{q_w} = 1 - \frac{H_{l,fdb} - H_l}{H_{l,fdb} - H_{l,OSV}} \tag{32}$$

where $H_{l,fdb}$ is the liquid enthalpy at the location where FDB is achieved. The FDB is assumed to occur when $\Delta T_{sub} \le \Delta T_{sub,fdb}$, where $\Delta T_{sub,fdb}$ is obtained from the Engelberg-Forster and Greif [44], as shown in Eq. (33).

$$\Delta T_{sub,fdb} = \frac{700 q_w}{h_{fc}} - 7.8 \exp\left[-0.0163(10P - 1)\right](700 q_w)^{0.25} \tag{33}$$

Fig. 16 presents the variation of the NBF along x_{th} under the same condition in Fig. 15. According to the modified Lahey model, q_b = 0 at the region upstream of OSV, and q_b = 1 at the region downstream of FDB. In the region of PB, forced convection and nucleate boiling both play a role. It should be noted that the modified Lahey model cannot predict the total wall heat flux by itself. Instead, the modified Chen model in Section 5.1.3 is used to predict the total wall heat flux.

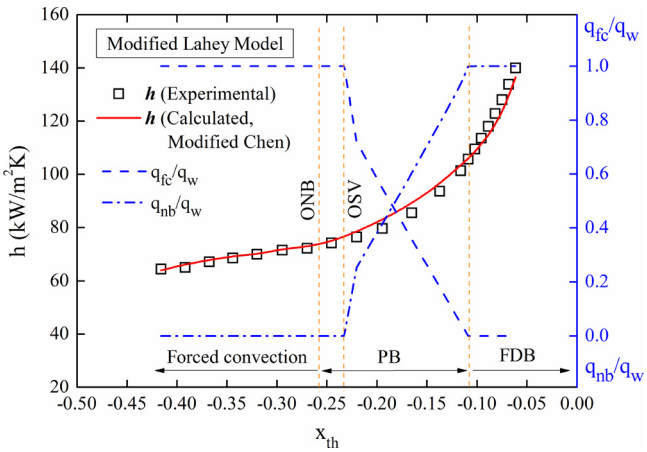

Fig. 16. Heat transfer coefficients and wall heat flux partitioning according to the modified Lahey model (P = 4.2 MPa, G = 10,000 kg/m^2 s, q = 7.5 MW/m^2).

6. Conclusions

Experimental investigations on subcooled water flow boiling in a vertical circular tube under HHHM conditions were carried out with respect to the ITER divertor cooling system. According to the experimental results, the following conclusions can be made.

(1) Heat transfer coefficients increase with an increase in mass flux and are little affected by heat flux and pressure in the SP region. In the region of nucleate boiling, heat transfer coefficients are mainly affected by heat flux and pressure and are almost independent of mass flux. A decrease in subcooling causes a decrease in ΔT_b and then an increase in heat transfer coefficients.

(2) A number of heat transfer correlations (seven correlations for FDB, four dimensionless correlations, and three Chen-type correlations) were compared with our experimental data. Most of these correlations cannot predict the experimental data with high accuracies. Thus, a modified Chen correlation was proposed to predict the total heat transfer coefficient under HHHM conditions. The modified Chen correlation can capture 97.07% data with an accuracy of ±15%, and its MAE and RMSE were 1.11% and 6.45%, respectively.

(3) Wall heat flux partitioning during subcooled flow boiling was also discussed. A modified Lahey model was proposed to predict the NBF in subcooled boiling under HHHM conditions. Note that the modified Lahey model cannot determinate the total wall heat flux by itself, and the modified Chen correlation mentioned above can be adopted to predict the total wall heat flux.

It should be noted that the modified Chen correlation proposed in this study cannot be directly used in one-sided heating applications. Further modifications, such as the approach proposed in Araki et al. [38], are required for one-sided heating applications. In addition, the present experiments were carried out only in a single test tube; therefore, the modified Chen correlation developed from these data is not general so far. More tests in different tube diameters and lengths are needed to assess its prediction performance and provide a more convincing conclusion.

Acknowledgment

This work is supported by MOST of China, No. 2011GB110001.

References

[1] G. Wang, P. Cheng, Subcooled flow boiling and microbubble emission boiling phenomena in a partially heated microchannel, Int. J. Heat Mass Transf. 52 (2009) 79–91.
[2] J. Lee, I. Mudawar, Critical heat flux for subcooled flow boiling in micro-channel heat sinks, Int. J. Heat Mass Transf. 52 (2009) 3341–3352.
[3] F. Dobran, Fusion energy conversion in magnetically confined plasma reactors, Prog. Nucl. Energy 60 (2012) 89–116.
[4] J. Milnes, A. Burns, D. Drikakis, Computational modelling of the HyperVapotron cooling technique, Fusion Eng. Des. 87 (2012) 1647–1661.
[5] A.R. Raffray, R. Nygren, D.G. Whyte, S. Abdel-Khalik, R. Doerner, F. Escourbiac, T. Evans, R.J. Goldston, D.T. Hoelzer, S. Konishi, P. Lorenzetto, M. Merola, R. Neu, P. Norajitra, R.A. Pitts, M. Rieth, M. Roedig, T. Rognlien, S. Suzuki, M.S. Tillack, C. Wong, High heat flux components – readiness to proceed from near term fusion systems to power plants, Fusion Eng. Des. 85 (2010) 93–108.
[6] K. Hata, S. Masuzaki, Subcooled boiling heat transfer in a short vertical SUS304-tube at liquid Reynolds number range 5.19×10^4 to 7.43×10^5, Nucl. Eng. Des. 239 (2009) 2885–2907.
[7] K. Hata, S. Masuzaki, Subcooled boiling heat transfer for turbulent flow of water in a short vertical tube, J. Heat Transf. Trans. ASME 132 (2010), 011501-011501-11.
[8] K. Hata, Y. Shirai, S. Masuzaki, Heat transfer and critical heat flux of subcooled water flow boiling in a HORIZONTAL circular tube, Exp. Therm. Fluid Sci. 44 (2013) 844–857.
[9] S.E.-D. El-Morshedy, A. Hassanein, Transient thermal hydraulic modeling and analysis of ITER divertor plate system, Fusion Eng. Des. 84 (2009) 2158–2166.
[10] S.E.-D. El-Morshedy, A. Hassanein, Analysis, verification, and benchmarking of the transient thermal hydraulic ITERTHA code for the design of ITER divertor, Fusion Eng. Des. 85 (2010) 687–693.
[11] J.C. Chen, A correlation for boiling heat transfer to saturated fluids in convective flow, Ind. Eng. Chem. Process Des. Dev. 5 (1966) 322–329.
[12] A. Ying, H. Zhang, D. Youchison, M. Ulrickson, 3D CFD analysis of subcooled flow boiling heat transfer with hypervapotron configurations for ITER first wall designs, Fusion Eng. Des. 85 (2010) 1348–1353.
[13] A. Kaya, M.R. Ozdemir, A. Kosar, High mass flux flow boiling and critical heat flux in microscale, Int. J. Therm. Sci. 65 (2013) 70–78.
[14] T. Cikim, E. Armagan, G.O. Ince, A. Kosar, Flow boiling enhancement in microtubes with crosslinked pHEMA coatings and the effect of coating thickness, J. Heat Transf. Trans. ASME 136 (2014), 081504-081504-11.
[15] W.M. Rohsenow, Chapter in Heat Transfer, University of Michigan Press, Ann Arbor, IL, 1953.
[16] J.G. Collier, Boiling within vertical tubes Heat Exchanger Design Handbook. Fluid Mechanics and Heat Transfer, vol. 2, Hemisphere, Washington, DC, 1984.
[17] A.E. Bergles, J.G. Collier, J.M. Delhaye, G.F. Hewitt, F. Mayinger, Two Phase Flow and Heat Transfer in the Power and Process Industries, MaGraw-Hill, New York, 1981, pp. 250.
[18] H.K. Forster, N. Zuber, Dynamics of vapor bubbles and boiling heat transfer, AIChE J. 1 (1955) 531–535.
[19] K.E. Gungor, R.H.S. Winterton, A general correlation for flow boiling in tubes and annuli, Int. J. Heat Mass Transf. 29 (1986) 351–358.
[20] M.G. Cooper, Saturation nucleate pool boiling, a simple correlation, in: First U.K. National Conference on Heat Transfer, 1984.
[21] Z. Liu, R.H.S. Winterton, A general correlation for saturated and subcooled flow boiling in tubes and annuli, based on a nucleate pool boiling equation, Int. J. Heat Mass Transf. 34 (1991) 2759–2766.
[22] Q.T. Zhou, Calculation of inner wall temperature for an electrically heated thick-wall tube, J. Nanjing Inst. Technol. 4 (1985) 38–43 (in Chinese).
[23] H.W. Coleman, W.G. Steele, Engineering application of experimental uncertainty analysis, AIAA J. 33 (1995) 1888–1896.
[24] V. Gnielinski, New equations for heat and mass transfer in turbulent pipe and channel flow, Int. Chem. Eng. 16 (1976) 359–368.
[25] S. Basu, S. Ndao, G.J. Michna, Y. Peles, M.K. Jensen, Flow boiling of R134a in circular microtubes – part I: study of heat transfer characteristics, J. Heat Transf. Trans. ASME 133 (2011), 051502-051502-9.
[26] C. Martin-Callizo, B. Palm, W. Owhaib, Subcooled flow boiling of R-134a in vertical channels of small diameter, Int. J. Multiphase Flow 33 (2007) 822–832.
[27] S. Saitoh, H. Daiguji, E. Hihara, Effect of tube diameter on boiling heat transfer of R-134a in horizontal small-diameter tubes, Int. J. Heat Mass Transf. 48 (2005) 4973–4984.
[28] M. Jamialahmadi, H. Muller-Steinhagen, H. Abdollahi, A. Shariati, Experimental and theoretical studies on subcooled flow boiling of pure liquids and multicomponent mixtures, Int. J. Heat Mass Transf. 51 (2008) 2482–2493.
[29] J.R.S. Thom, W.M. Walker, T.A. Fallon, G.F.S. Reising, Boiling in subcooled water during flow up heated tubes or annuli, Proc. Inst. Mech. Eng. 180 (1966) 226–246.
[30] A.V. Dedov, A.T. Komov, A.N. Varava, V.V. Yagov, Hydrodynamics and heat transfer in swirl flow under conditions of one-side heating. Part 2: boiling heat transfer. Critical heat fluxes, Int. J. Heat Mass Transf. 53 (2010) 4966–4975.
[31] M.M. Shah, A general correlation for heat transfer during subcooled boiling in pipes and annuli, ASHRAE Trans. 82 (1976) 66–86.
[32] S.G. Kandlikar, Heat transfer characteristics in partial boiling, fully developed boiling, and significant void flow regions of subcooled flow boiling, J. Heat Transf. Trans. ASME 120 (1998) 395–401.

[33] S.S. Papel, Subcooled Boiling Heat Transfer Under Forced Convection in a Heated Tube, Technical Note D-1583, NASA, Cleveland, OH, 1963.
[34] M. Badiuzzaman, Correlation of subcooled boiling data, Pak. Eng. 7 (1967) 759–764.
[35] F.D. Moles, J.F.G. Shaw, Boiling heat transfer to subcooled liquids under condition of forced convection, Trans. Inst. Chem. Eng. Chem. Eng. 50 (1972) 76–84.
[36] P.K. Baburajan, G.S. Bisht, S.K. Gupta, S.V. Prabhu, Measurement of subcooled boiling pressure drop and local heat transfer coefficient in horizontal tube under LPLF conditions, Nucl. Eng. Des. 255 (2013) 169–179.
[37] V. Prodanovic, D. Fraser, M. Salcudean, Bubble behavior in subcooled flow boiling of water at low pressures and low flow rates, Int. J. Multiphase Flow 28 (2002) 1–19.
[38] M. Araki, M. Ogawa, T. Kunugi, K. Satoh, S. Suzuki, Experiments on heat transfer of smooth and swirl tubes under one-sided heating conditions, Int. J. Heat Mass Transf. 39 (1996) 3045–3055.
[39] P. Griffith, J.A. Clark, W.M. Rohsenow, Void volumes in subcooled boiling, ASME Paper 58-HT-19, in: U.S. National Heat Transfer Conference, Chicago, 1958.
[40] R.W. Bowring, Physical Model Based on Bubble Detachment and Calculation of Steam Voidage in the Subcooled Region of a Heated Channel, HPR-10, Institute for Atomenergi, Halden, Norway, 1962.
[41] S.Z. Rouhani, E. Axelsson, Calculation of void volume fraction in subcooled and quality boiling regions, Int. J. Heat Mass Transf. 13 (1970) 383–393.
[42] W.T. Hancox, W.B. Nicoll, General technique for prediction of void distributions in non-steady 2-phase forced convection, Int. J. Heat Mass Transf. 14 (1971) 1377–1394.
[43] P. Saha, N. Zuber, Point of net vapor generation and vapor void fraction in subcooled boiling, in: Proceedings of the 5th International Heat Transfer Conference, Tokyo, Japan, vol. 4, Hemisphere Publishing Corporation, Washington, 1974, pp. 175–179.
[44] K. Engelberg-Forster, R. Greif, Heat transfer to a boiling liquid-mechanism and correlation, Trans. ASME Ser. C: J. Heat Transf. 81 (1959) 43–53.
[45] W.H. Jens, P.A. Lottes, Analysis of Heat Transfer Burnout Pressure Drop, and Density Data for High Pressure Water, ANL-4627, 1951.
[46] D.A. Labuntso, Heat-transfer problems with nucleate boiling of liquids, Therm. Eng. 19 (1972) 21–28.